

Influence of electrostatic charges on the particle concentration in wall-bounded turbulent flows

H. Grosshans^{a,*}, L. Villafañe^b, A. Banko^b, M.V. Papalexandris^c

^a*Physikalisch-Technische Bundesanstalt (PTB), Bundesallee 100, 38116 Braunschweig, Germany*

^b*Department of Mechanical Engineering, Stanford University, CA*

^c*Institute of Mechanics, Materials and Civil Engineering, Université catholique de Louvain, 1348 Louvain-la-Neuve, Belgium*

Abstract

Preferential concentration of inertial particles in wall-bounded turbulent flows is of paramount importance and, thus, subject of fundamental research. In practical applications of confined particle-laden flows the particles experience frequent collisions with the piping system which may result in an unwanted electric charge separation through triboelectric effects. The consequential occurrence of electrostatic forces alters the particle trajectories and, thus, impairs the general validity of the measured results to an unknown extent. In this work the influence of triboelectric charging on the preferential concentration of inertial particles in a fully developed turbulent duct flow was investigated by means of a combined numerical and experimental approach. The order of magnitude of the potential charge accumulation was estimated and imposed in a parametric study to the particulate phase in the simulations. The simulations demonstrate that the concentration profiles are for the most part independent of the prescribed charge. However, the peaks of the particle number density at the walls caused by turbophoresis are strongly reduced through the local increase of repelling electrostatic forces. The comparison of numerical with experimental data indicates that the particles in the experimental setup are affected by a surface charge density of the order of $40 \mu\text{C}/\text{m}^2$. The presented results aim to elucidate the impact of electrostatic forces in the particle distribution in wall-bounded particle-laden flows.

Keywords: electrostatics, particle dynamics, particulate flows, experiment, simulation

Introduction

Preferential concentration of inertial particles in fully-developed wall-bounded turbulent flows is of relevance to many industrial applications, such as pneumatic powder conveying [1], pulverized coal combustion [2] or particle-based solar receivers [3]. For this reason, this type of flows is subject to experimental research since decades. Noteworthy classical works include those by Tsuji and Morikawa [4], Tsuji et al. [5] who collected a large set of data concerning the mean velocity

*Corresponding author

Email address: holger.grosshans@ptb.de (H. Grosshans)

of powders in vertical and horizontal flows through circular pipes. This kind of experimental study requires the usage of a long feed-line in order to obtain a fully-developed flow at the test section and to ensure that the particles are independent of their initial conditions. However, as the particles are advected along the piping system they may experience frequent collisions with the walls and between each other. If the powder and the piping system are of a different kind of material their contact results in an electric charge separation through triboelectric effects [6]. Under those circumstances a considerable amount of electric charge might be accumulated on the surface of the particles or on the structural components of the facility.

One easily observable consequence is the deposition of particles on the surfaces of the test section [7, 8, 9]. If no adequate measure is taken, such as the usage of an antistatic agent (as done by Tsuji and Morikawa [4], Tsuji et al. [5]), particle deposition might alter near-wall particle concentrations. Also, deposition layers may induce detrimental effects on the experiments, i.e., constrain optical access and light transmission. Another, less obvious, implication of electrostatic forces is the modulation of the particle trajectories of airborne particles. In an experimental setting, the exact influence of electrostatics on the measured particle concentration statistics is unknown. Moreover, in an industrial context the formation of deposits can impair the functionality of the facilities by reducing the effective cross-sectional area of pipes. Also, excessive local charge accumulation can effectuate sparks which challenges the operational safety of a plant [10, 11, 12].

Experimental measurements in the near-wall region in particle-laden flows are challenging due to the wall interference with optical measurement techniques, and also because of the temporal and spatial resolution required to capture the small scales of the particle and flow structures of interest. Limited data is available of gas and particle phase statistics near walls [13]. Measurements are often restricted to a certain parameter range due to experimental limitations, i.e. relatively large small flow scales to be able to measure all fluid fluctuations, or particle diameters larger than the dominant near-wall eddies [14]. Conversely, numerical simulations have been extensively used to study near wall phenomena. A remarkable early contribution was the ability of capturing the accumulation of particles in the viscous sublayer through *turbophoresis*, i.e. the tendency of particles to migrate in the direction of decreasing turbulent intensity, by means of direct numerical simulations (DNS) [15, 16]. More recent examples include the explanation of the mechanisms for particle transfer in the turbulent boundary layer by Marchioli and Soldati [17] and the computation of the inertial migration of particles in laminar square duct flow by Tabaei Kazerooni et al. [18]. Nonetheless, simulations rarely consider the possible effect of arising electrostatic forces which are expected in real particle-laden flows.

Previous numerical works proposing approaches to predict the charge build-up process of solid-fluid mixtures incorporated different levels of simplifications. For example, the simulations by Hogue et al. [19] described the charging of particles but neglected the influence of aerodynamic forces on their trajectories. Watano et al. [20] included drag forces in the numerical framework but they assumed the gaseous phase to follow a predefined velocity profile, i.e. the interaction between particle dynamics and turbulence was not accounted for. The same counts for the studies of Kolniak and Kuczynski [21] and Tanoue et al. [22, 23] who solved the Reynolds-Averaged Navier-Stokes equations for the turbulent gas flow. The fluid-particle interaction was computed through large-eddy simulations (LES) by Lim et al. [24]. However, they focused on the influence of an external electric field on already charged particles. The authors of the present paper implemented

dynamic models to predict the contact charging of particles when colliding with a solid surface or with each other into a computational fluid dynamics solver. Employing this computational framework generic geometries such as channel and pipe flows were studied while accounting by DNS [25] or LES [26] for the turbulence of the carrier fluid. Albeit electrical forces were included in the set of equations, the size of the flown-through vessels was small, i.e. the initial charge build-up was evaluated. Therefore, the accumulated charge was rather low and did not significantly influence particle dynamics.

To sum up, the influence of accumulated electrostatic charge on the preferential concentration of particles in wall-bounded flows in large-scale facilities is not known to date. While experimental results may be affected by electrostatic forces, quantification of the precise impact is at present lacking. In order to evaluate its contribution we investigated the influence of triboelectric charging on inertial particles in a fully-developed, vertical, turbulent duct flow by comparison of numerical and experimental results. In the following section of this paper the experimental facility is presented followed by an outline of the numerical methodology. Results are discussed in the fourth section followed by the main conclusions from the present study.

Experimental methods

Experimental data was obtained in a square section duct flow facility at Stanford University, see Villafañe et al. [27]. A 5.4 m long smooth aluminum duct with a 40 mm wide cross section ensures a fully developed turbulent air flow at the glass test section where measurements are

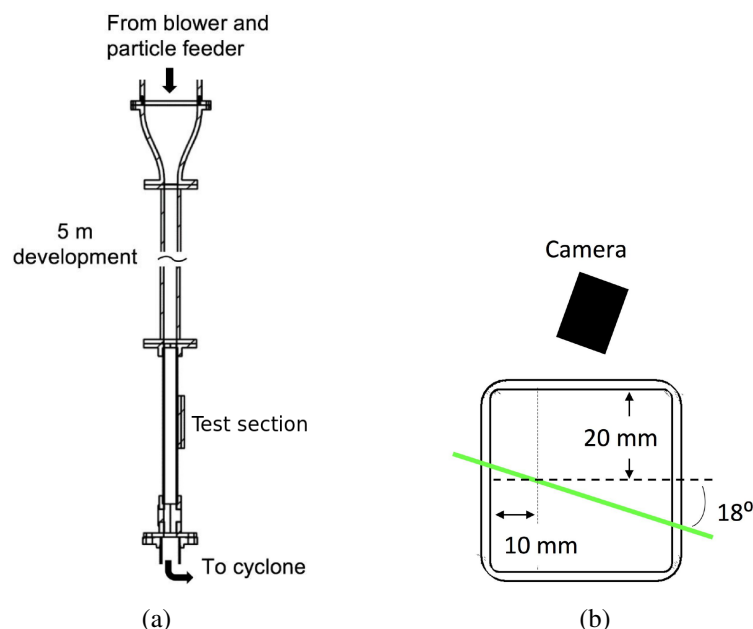


Figure 1: Experimental apparatus: (a) layout of the particle-laden duct flow facility, (b) laser sheet configurations used for measurements of mean particle concentration [27].

reported. An schematic of the vertical rig is shown in figure 1(a). A variable speed centrifugal pressure blower controls the inlet air flow to sustain a constant Reynolds number during the tests. A volumetric screw feeder is used to feed the particles into a flow conditioning section with a cross section 16 times larger than that of the main flow duct. Several grids placed downstream of the particle injection help to laterally disperse the particles prior to the contraction between the flow conditioning unit and the development duct section. The test section consist on a 425 mm long borosilicate glass duct with a nominal internal cross-section of 40 mm \times 40 mm, and 2 mm thick walls. The test section was manufactured by extrusion to eliminate the presence of joints. The manufacturing process is responsible for the 2 mm internal corner radii in the test section cross section that limits the optical accessibility to the near wall region along the wall normal direction. Figure 1(b) illustrates the test section cross section and the optical set-up configuration used to measure particle concentration profiles in the vicinity to the wall. Downstream of the test section the particles are separated from the air and collected at a cyclone, and the air flow is exhausted to the atmosphere.

Planar measurements of mean particle concentration were performed at a Reynolds number based in the duct width and bulk flow velocity of $Re = 10\,000 \pm 0.7\%$. The nickel particles used have a number-based mean diameter of $11.8 \pm 0.5 \mu\text{m}$. The particle-size distribution shown in figure 3 is characterized by low probability tails covering a range from 6 μm to 20 μm . Particle size distributions before and after the tests were measured by a Coulter Counter and confirmed that particles were not selectively filtered by the rig. An average Stokes number of $St_\eta = 5$ corresponds to the experimental particle and flow parameters. The average Stokes number is based on the mean particle diameter and the Kolmogorov flow time scale derived from the channel-averaged dissipation rate. A ratio of particle to gas mass loading of 0.01 was imposed in the experiments, with a maximum uncertainty of 0.004.

Particle velocity and concentration measurements were performed using planar optical techniques, i.e. a collimated laser sheet from a pulsed NdYag laser crossing the test section with a constant thickness and width, and a high resolution CCD camera normal to it. A set of 4 cylindrical lenses were used to form a laser sheet with a $1/e^2$ Gaussian beam thickness of 1.6 mm and a width of 25 mm. The angled laser sheet configuration shown in figure 1(b) was adopted to measure the concentration distribution near the wall. The laser sheet is inclined 18° with respect to the wall-normal and crosses the central plane of the test section at 10 mm from the wall. The high resolution camera synchronized with the pulsed laser acquired time independent images of the particles within the laser sheet. Image processing algorithms were used to identify individual particles in 2000 independent images, and extract the two-dimensional coordinates of particle centroids that were used to compute concentration profiles.

Mathematical model and numerical methods

This section summarizes the CFD solver which was employed in the present study. This solver utilizes a four-way coupled approach where the continuous gaseous phase is described in Eulerian and the dispersed particulate phase in Lagrangian framework [28]. In the gaseous phase model given by Grosshans and Papalexandris [26, 25] the flow is considered dilute so the volume fraction

of the gaseous phase can assumed to be unity. Thus, the mass and momentum balance laws are given by the Navier-Stokes equations with constant diffusivities, namely

$$\nabla \cdot \mathbf{u} = 0 \quad (1a)$$

$$\frac{\partial \mathbf{u}}{\partial t} + (\mathbf{u} \cdot \nabla) \mathbf{u} = -\frac{1}{\rho} \nabla p + \nu \nabla^2 \mathbf{u} + \mathbf{F}_s + \mathbf{F}_f. \quad (1b)$$

In the above equations \mathbf{u} denotes the gas velocity, p its pressure, ρ its density and ν its kinematic viscosity. A source term, \mathbf{F}_s , accounting for the momentum transfer from the particulate to the gaseous phase is also introduced. The flow is forced in positive x -direction by adding a constant pressure gradient, \mathbf{F}_f .

The governing equations of LES are obtained by applying a spatial filter operator to equations (1a) and (1b). Thus, the large-scale turbulent motions are directly resolved on the computational grid. On the other hand, the small sub-filter scales, which exhibit universal characteristics, are considered through an appropriate turbulence model. To this end, the implicit model by Boris et al. [29] is applied. The above Eulerian equations are discretized by the Finite Difference Method (FDM). In particular, the convective terms are approximated by an up to fifth-order Weighted Essentially Non Oscillatory (WENO) scheme [30]. The diffusive and pressure terms are approximated by fourth-order central differences and the time derivatives by an implicit second-order backward scheme. For further details concerning the numerical implementation the reader is referred to Gullbrand et al. [31].

The particulate phase is treated according the numerical methodology proposed by Grosshans and Papalexandris [32] and implemented by [33]. This methodology is extended to facilitate the treatment of a large amount of particles as outlined in the following. In the current setting, the particle probability density function is given by

$$\zeta = \zeta(\mathbf{u}_p, r_p, Q_p; \mathbf{x}, t). \quad (2)$$

This expression gives the probable number of particles having a velocity of \mathbf{u}_p , a radius of r_p and carrying an electrical charge of Q_p at a certain location, \mathbf{x} , and time instance t . In order to handle the large amount of particles the stochastic parcel method [34] is adopted to approximate ζ . Accordingly, the above function is discretized in computational parcels, each parcel representing $\zeta = 10$ particles, which each is tracked in a Lagrangian framework.

The trajectory of a parcel is altered by accelerations due to aerodynamic, \mathbf{f}_{ad} , collisional, \mathbf{f}_{coll} , gravitational, \mathbf{f}_g , and electric field, \mathbf{f}_{el} forces. As regards the aerodynamic acceleration the particle drag coefficient is derived as a function of the particle Reynolds number following the classical correlation of Schiller and Naumann [35]. Furthermore, gravitation accelerates the particles towards the positive x -direction.

With respect to acceleration during collisions, binary particle collisions and elastic reflection of the particles off the walls is accounted for. To enhance computational efficiency, a statistical technique that yields a collision frequency is employed [36]. More specifically, it is assumed that the probability P_n that the particles of parcel n collide with the particles of parcel m during the time increment dt follows a Poisson distribution, namely

$$P_n = 1 - e^{-\omega_{nm} dt}. \quad (3)$$

In this equation, the time-averaged collision frequency ω_{nm} is defined as

$$\omega_{nm} = \pi \frac{\zeta_m (r_{p,n} + r_{p,m})^2 |\mathbf{u}_{p,n} - \mathbf{u}_{p,m}|}{(\mathbf{e}_x \cdot \boldsymbol{\delta})(\mathbf{e}_y \cdot \boldsymbol{\delta})(\mathbf{e}_z \cdot \boldsymbol{\delta})} \quad (4)$$

where $\boldsymbol{\delta}$ is a vector pointing from the location of one parcel to the other, \mathbf{e}_x , \mathbf{e}_y and \mathbf{e}_z denote the unit vectors of the Cartesian coordinate system and \cdot the scalar product.

As regards electrostatic forces, the specific force acting on a particle due to the electric field is calculated as

$$\mathbf{f}_{el} = \frac{Q_p \mathbf{E}}{m_p} \quad (5)$$

where m_p is the mass of the particle. Concerning the computation of the electric field strength, \mathbf{E} , there are two different approaches available, namely Gauss' and Coulomb's law. In the present study, a computational efficient and accurate hybrid scheme which combines both approaches which was proposed by Grosshans and Papalexandris [32] is applied. Therein, the interaction of an individual particle with the space charge, i.e. with the electric field originating from the particle cloud, is calculated by Gauss' law. Furthermore, the derivation of the forces between particles located close to each other (here: present in the same grid cell) is based on Coulomb's law.

According to Gauss' law, the divergence of the electric field is related to the electric charge density per unit volume, ρ_{el} , by

$$\nabla \cdot \mathbf{E} = \frac{\rho_{el}}{\varepsilon}. \quad (6)$$

In the above equation $\varepsilon = 8.854 \text{ F/m}$ denotes the electrical permittivity of the vacuum and ρ_{el} is defined as

$$\rho_{el} = \left((\mathbf{e}_x \cdot \boldsymbol{\nu})(\mathbf{e}_y \cdot \boldsymbol{\nu})(\mathbf{e}_z \cdot \boldsymbol{\nu}) \right)^{-1} \int_{\boldsymbol{\nu}} \zeta Q \, d\mathbf{x} \quad (7)$$

where $\boldsymbol{\nu}$ is the unit volume.

For the case of charged particles, alternatively Coulomb's law can be used, i.e.

$$\mathbf{E}(\mathbf{r}) = \frac{\zeta_m Q_m \mathbf{r}}{4 \pi \varepsilon |\mathbf{r}|^3}. \quad (8)$$

Therein, $\mathbf{E}(\mathbf{r})$ is the electric field a particle is subjected to due to the presence of another parcel at a distance of \mathbf{r} consisting of ζ_m particles carrying the charge Q .

Whereas Gauss' and Coulomb's law are mathematically equivalent, the numerical methods for solving them when dealing with a large number of particles may differ considerably in terms of accuracy and computational costs. For the proof of their equivalence and a detailed discussion concerning the advantages and disadvantages of each approach, the reader is referred to Grosshans and Papalexandris [32].

As regards the numerical set-up, in streamwise direction, the computational domain extends $15 H$. Further, periodic boundary conditions are chosen in streamwise direction in order to mimic an infinite duct length and no-slip is assumed for the gaseous phase at the sidewalls. Consistent to the experiments, a duct flow of $Re = 10\,000$ was considered. Moreover, the particle size

distribution, which is detailed in the following section, replicates the utilized powder. The duct is defined to be bounded and manufactured of a conductive material. This choice implies that an electrical charge which might be brought to the ducts surface upon contact with a particle, vanishes almost instantly towards ground. Nonetheless, a so-called image charge is accounted for at the surface if a charged particle residing in its vicinity. Aiming to obtain efficiently results for long averaging times, a rather coarse numerical grid was applied. Namely, the first grid point was placed at a distance of $y^+ = 6$ from the wall which results in a total number of 1.2 million points.

Results and discussion

Code validation

The above Eulerian-Lagrangian solver has been applied previously to simulate a wide range of dispersed flows such as LES and DNS of pneumatic powder conveying [26, 37, 38, 39, 9, 25]. The mentioned references include a large amount of validation studies of various aspects of the solver, realized e.g. through grid resolution studies and comparison with experiments. In particular, the implementation of the dynamics of charged particles in the influence of an electric field was validated in Ref. [32].

Specifically for the current set-up the implementation of the Eulerian solver for the fluid phase has been validated by Grosshans [33] through comparison of the solution for a single-phase flow with the DNS data of Zhu et al. [40] which was also performed for a duct flow of $Re = 10\,000$ and the empirical law of the wall [41] and log-law [42]. The profiles of the mean streamwise velocity component, i.e. averaged in time and in the homogeneous streamwise direction and normalized to the friction velocity u_τ , compare very well with the earlier DNS and to an expected degree with the empirical laws.

Further, the profiles of the root-mean-square (r.m.s.) fluctuations of the three velocity components are plotted in figure 2. These and the following results are given in terms of wall units,

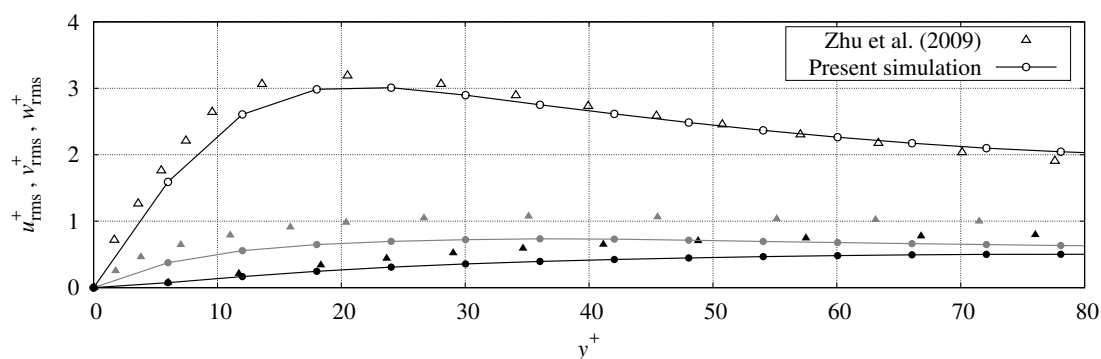


Figure 2: Profiles of r.m.s. velocity fluctuations for a single-phase flow. Comparison of our numerical results with the DNS data of Zhu et al. [40]. The empty symbols denote the streamwise velocity component u_{rms}^+ , the black symbols the wall-normal component v_{rms}^+ , and the grey symbols the spanwise velocity component w_{rms}^+ [33].

$y^+ = u_\tau y/\nu$. In general, good agreement to the DNS data of Zhu et al. [40] is ascertained. However, in comparison the turbulent fluctuations predicted by our simulations are of a lower amplitude. This can be explained by the relative coarse grid employed for the computations which impedes the resolution of the smallest flow scales in the viscous wall region ($y^+ < 50$) where the production of turbulent kinetic peaks [43]. Nevertheless, the curves agree sufficiently to provide qualitatively reliable results.

Initial particle charge

The expected charge of the particles at the glass test section inlet is imposed as an initial condition in the simulations and varied systematically. By doing so, the effect of electrostatic charge accidentally aggregated by the particles on their preferential concentrations in the experimental apparatus is evaluated. For this purpose first the order of magnitude of the potential amount of charge carried by the particles when reaching the test section is estimated. This estimation serves as a basis for the decision on the parameter range to be investigated. With respect to the methodology for the evaluation, we compare the maximum charge predicted by the charging model implemented by

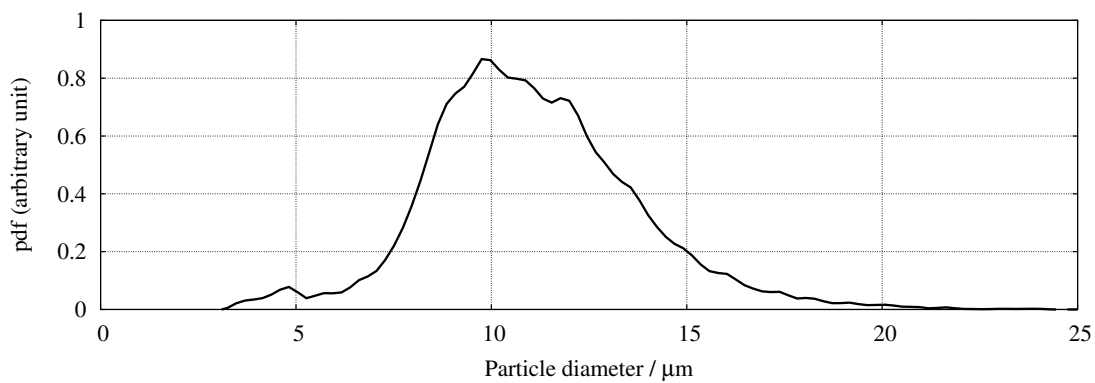


Figure 3: Particle size distribution measured with a Coulter Counter and replicated in the simulations.

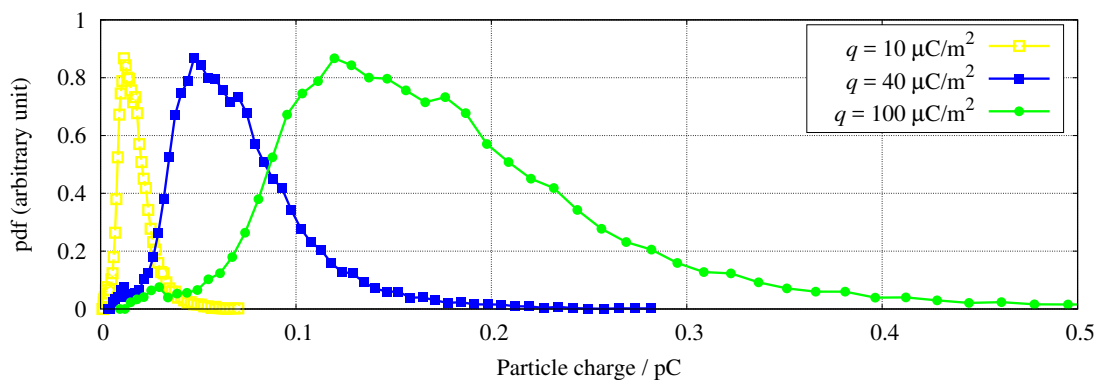


Figure 4: Charge distributions assigned to the particles in the simulations.

Grosshans and Papalexandris [25] with the outcome of the charge relaxation model by Matsuyama [46].

As regards the former approach, it is assumed that the charge originates from triboelectric effects during collisions of the particles with structural components such as the blower, feeder or duct walls (cf. figure 1(a)) prior to the test section. Whereas the amount of collisions taking place is unknown one can utilize the dynamic model implemented by Grosshans and Papalexandris [25] to predict an order of magnitude of the maximum charge a particle can obtain. This charge value is also termed equilibrium charge, since for further collisions the amount of pre-charge transferred from the particle to the surface equals the triboelectric charge separation, i.e. the net charge transfer is zero. Following this model, even though the total equilibrium charge depends on the particle size, the equilibrium surface charge density, q_{eq} is independent. More precisely, for a theoretically infinite number of collisions the model predicts an asymptotic limit for q of

$$q_{\text{eq}} = \frac{\varepsilon U}{h}. \quad (9)$$

In this equation U denotes the contact potential and h the particle-surface separation distance. Consulting the well-known triboelectric series [e.g. 44] one may assume a value of the order of 1 V for the contact potential. Concerning h , a commonly used estimate relates to the order of the range of repulsive molecular forces due to surface irregularities, namely $h = 10^{-9}\text{m}$ [45, 21, 26]. These assumptions lead to a maximum charge density of $q_{\text{eq}} = 8.85 \times 10^{-3} \text{ C/m}^2$.

Nonetheless, as recently discussed by Matsuyama [46] such a high value cannot be obtained in reality since a charge relaxation takes place immediately after the particle-surface contact. This relaxation occurs due to discharge at the contact gap when the potential difference equals the gaseous breakdown limit potential. Thus, this mechanism limits the maximum charge a particle can carry. Matsuyama [46] compared in his work the prediction of the breakdown limit potential by Paschen's law with their impact charging experiments of single particles [cf. 47, 48, 49]. The compared data set indicate that a particle of the size of 12 μm , which corresponds to the mean particle size in the present study, is able to carry a maximum charge of about 0.5 pC or, in other words, a surface charge density of about $q = 10 \mu\text{C/m}^2$.

Considering the discussion provided above, we assigned a constant charge density to the particles during each simulation. First, for comparison purposes one simulation with an uncharged particulate phase was ran. Further, four cases with different charge density values, namely $q = 10 \mu\text{C/m}^2$, $q = 40 \mu\text{C/m}^2$ and $q = 100 \mu\text{C/m}^2$, were computed. In other words, a parameter space which includes uncharged particles, particles carrying a charge which corresponds to the limit predicted by the charge relaxation model and up to ten times the respective value was explored. This choice aims to give an overview over the flow pattern to be expected in this type of flows. However, it is noted that several underlying assumptions which may not coincide with the realistic conveying situation. These include the assumption of homogeneously distributed charge on the surface of each particle which might not be reachable considering the finite number of collisions of the particle with the test rig. Further, the charge of particulate phase might be dependent on the distance to the wall, i.e. a particle close to the wall is expected to accumulate more charge than a particle in the bulk of the flow.

A consequence of the decision to assign a constant surface charge density is the dependence of the total particle charge on its size. The particle size distribution measured before the experiment and replicated in the simulations is plotted in figure 3. The resulting particle charge distributions when applying the surface charge densities in the simulations are given in figure 4.

Particle concentrations

In the simulations an initially fully-developed turbulent flow field was considered. The particles were introduced at random positions whereas their initial velocity was assumed to equal the local velocity of the surrounding fluid. The resulting mean concentration profiles along the laser sheet centerline normalized by the mean concentration at $y = 0.05 H$ are plotted for the near-wall region in figure 5. Since the planar laser sheet was inclined by 18° with respect to the wall-normal (cf. figure 1(b)) the z^+ position varies with the y^+ coordinate.

The differences in the presented numerical results reveal the potential influence of electrostatic charges on preferential particle concentration. Apparently, the effect of the electrostatic charges on the particle concentrations is most pronounced in the vicinity of the wall, i.e. in the region $y^+ < 15$. Comparing the different numerical data suggests that the case corresponding to $q = 40 \mu\text{C}/\text{m}^2$ replicates the closest the experimental measurements. The proximity of both curves indicates that the powder utilized in the experiment might be subjected to a charge of this respective order of magnitude. However, a full compliance between experiments and simulations cannot be expected from the present study. On the one hand this discrepancies can be attributed to inaccuracies in the numerical methodology, namely the rather crude assumptions underlying the charge distribution which have been discussed in the previous subsection and the limited resolution of the turbulent flow scales in the simulations (cf. figure 2). Also the boundary conditions to the electric field may play a role: while in the simulations the wall is considered to be conductive and grounded, the corresponding components in the experimental facility consist of a mix of materials including

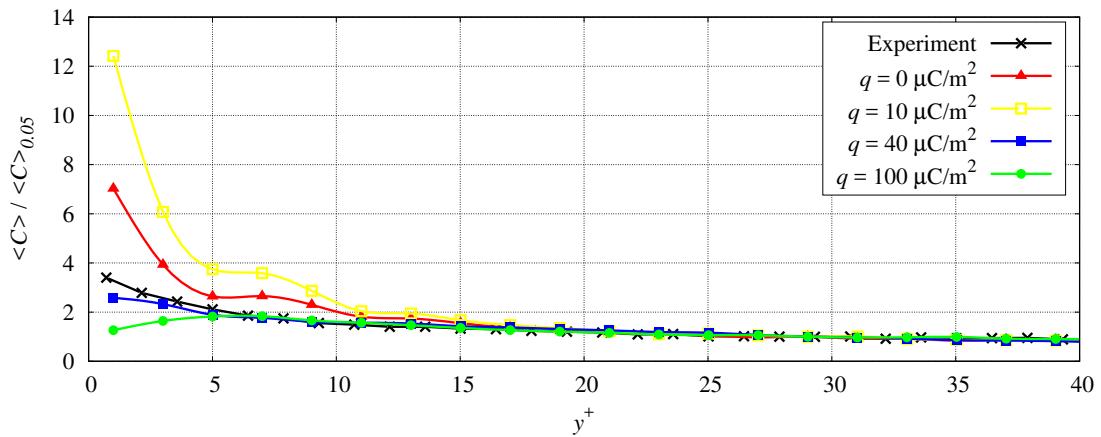


Figure 5: Comparison of the measured and simulated mean particle concentration distribution in the near-wall region. The local concentration is normalized by the mean concentration at $y = 0.05 H$. Note that the plotted data is collected along the laser beam (cf. figure 1(b)), i.e. the respective z^+ position varies with the y^+ coordinate.

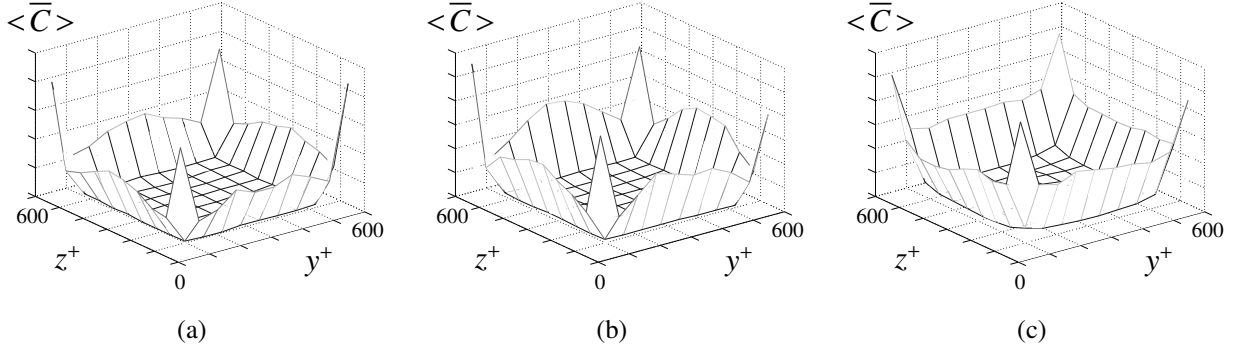


Figure 6: Normalized mean particle concentration in arbitrary units, $\langle \bar{C} \rangle$, over the duct cross-section. The particles carry a surface charge density q of (a) $0 \mu\text{C}/\text{m}^2$, (b) $10 \mu\text{C}/\text{m}^2$ and (c) $40 \mu\text{C}/\text{m}^2$

grounded metal parts but also glass. On the other hand there are few differences in the data acquisition. In the numerical post-processing procedure all particles are counted whose center point resides within the thickness of the laser sheet. In contrast, the laser beam in the experiments is of a Gaussian intensity profile which decreases the probability to detect small particles at the beam flanks. Further, due to the laser thickness being much larger than the particle diameter, particles may overlap and not be detected.

All the profiles presented in figure 5 indicate the effect of turbophoresis, i.e. particle accumulation in the near wall region. Comparing the numerical data related to the uncharged case with $q = 40 \mu\text{C}/\text{m}^2$ and $q = 100 \mu\text{C}/\text{m}^2$ shows that the peak at the wall reduces with increasing particle charges. This behavior was observed before [33] and attributed to the increasing electrostatic forces between particles. These forces are most prominent in regions of a high particle number density since there the average spacing between particles is the lowest. Consequently, particles are pushed out of the near-wall region towards the bulk of the flow. In other words, electrostatic charges tend to smoothen the particle concentration profiles.

Nonetheless, the profile related to $q = 10 \mu\text{C}/\text{m}^2$ in figure 5 evolves contradictory to this argumentation. Surprisingly, the concentration of this case peak at the wall higher than for the uncharged particles. To get further insight the mean particle concentrations over the complete duct cross-section are depicted in figure 6. On the whole, the particle accumulation close to the walls can be observed for all cases. In particular, the distributions relating to the uncharged particles (figure 6(a)) exhibit the strongest peaks at the four corners of the duct. Additional maxima are formed at the centerlines of the four sidewalls. These characteristic peaks in the ducts corner and sidewalls centerlines are qualitative agreement with the observations of Noorani et al. [50] and Tabaei Kazerooni et al. [18].

When the charge density is increased to $q = 10 \mu\text{C}/\text{m}^2$ (figure 6(b)) the particles are forced to migrate from the regions of highest accumulation, i.e. the duct corners. Nevertheless, instead of migrating to the bulk of the flow they travel along the sidewalls and feed the peaks at their centerline. Since the profiles in figure 5 depict locations close to the sidewall centerlines, this motion explains the rise of the particle concentration for $q = 10 \mu\text{C}/\text{m}^2$. If the charge density is

further increased to $q = 40 \mu\text{C}/\text{m}^2$ (figure 6(c)), the forces between the particles residing in these regions becomes high and, thus, the peaks are smoothed out. Consequently, the maximum of the related profile in figure 5 at the wall reduces. For a further increase to $q = 100 \mu\text{C}/\text{m}^2$, the particle behavior is qualitatively similar to the case of $q = 40 \mu\text{C}/\text{m}^2$, but the electrostatic forces affect an even stronger smoothing of the concentrations. Therefore, for $q = 100 \mu\text{C}/\text{m}^2$ only a slight particle accumulations is detectable in the region $0 < y^+ < 10$.

Conclusions

We examined the role of accidentally accumulated electrostatic charge in the mean particle concentration distribution and in particular in the near wall increase of concentration due to turbophoresis. Numerical simulations of particles of equal polarity in a fully developed duct flow were performed considering a homogeneous charge density on the particles' surface. Whereas the simulations reproduced the particle size distribution measured in the experiments the charge density was varied systematically. The resulting concentration profiles were compared to experimental data for which the particle charge is unknown. The numerical parametric study reveals that electrostatic charges play an important role in the particle redistribution, especially in the near wall region. In general, the simulations corroborate that the electrical forces tend to smoothen the particle concentration profiles, i.e. counteract particle accumulation through turbophoresis. The numerical results for a surface charge density of $40 \mu\text{C}/\text{m}^2$ are the closest to the experimental data. A future elaboration of this topic requires the simulation of the charge build-up process in order to get a more realistic picture of the charge distribution of the powder, as well as higher resolution of the small flow scales.

Acknowledgments

HG gratefully acknowledges the financial support from the Max Buchner Research Foundation. LV and AB gratefully acknowledge the funding by the Advanced Simulation and Computing (ASC) program of the US Department of Energys National Nuclear Security Administration via the PSAAP-II Center at Stanford, Grant No. DE-NA0002373-1. MP gratefully acknowledges the financial support of the National Research Fund of Belgium (FNRS) under the GRANMIX Projet de Recherche grant.

References

- [1] S. S. Grossel. Design and Operating Practices for Safe Conveying of Particulate Solids. *J. Loss Prev. Process Ind.*, 25:848–852, 2012.
- [2] J. G. M. Kuerten, C. W. M. van der Geld, and B. J. Geurts. Turbulence modification and heat transfer enhancement by inertial particles in turbulent channel flow. *Phys. Fluids*, 23(12): 123301, 2011.
- [3] Andrej Lenert and Evelyn N. Wang. Optimization of nanofluid volumetric receivers for solar thermal energy conversion. *Sol. Energy*, 86(1):253 – 265, 2012.
- [4] Y. Tsuji and Y. Morikawa. LDV measurements of an air-solid two-phase flow in a horizontal pipe. *J. Fluid Mech.*, 120:385–409, 1982.

- [5] Y. Tsuji, Y. Morikawa, and H. Shiomi. LDV measurements of an air-solid two-phase flow in a vertical pipe. *J. Fluid Mech.*, 139:417–434, 1984.
- [6] S. L. Soo. Dynamics of Charged Suspensions. In *Topics in Current Aerosol Research*, pages 71–73. Pergamon Press, 1971.
- [7] I. Adhiwidjaja, S. Matsusaka, S. Yabe, and H. Masuda. Simultaneous phenomenon of particle deposition and reentrainment in charged aerosol flow – effects of particle charge and external electric field on the deposition layer. *Adv. Powder Technol.*, 11(2):221–233, 2000.
- [8] J. Guardiola, V. Rojo, and G. Ramos. Influence of particle size, fluidization velocity and relative humidity on fluidized bed electrostatics. *J. Electrostat.*, 37(1–2):1–20, 1996.
- [9] N. Schwindt, U. von Pidoll, D. Markus, U. Klausmeyer, M. V. Papalexandris, and H. Grosshans. Measurement of electrostatic charging during pneumatic conveying of powders. *J. Loss Prev. Process Ind.*, 49:461–471, 2017.
- [10] M. Glor. Ignition hazard due to static electricity in particulate processes. *Powder Technol.*, 135–136:223–233, 2003.
- [11] W. Fath, C. Blum, M. Glor, and C.-D. Walther. Electrostatic ignition hazards due to pneumatic transport of flammable powders through insulating or dissipative tubes and hoses – new experiments and calculations. *J. Electrostat.*, 71(3):377–382, 2013.
- [12] S. Egan. Learning lessons from five electrostatic incidents. *J. Electrostatics*, 88:183–189, 2017.
- [13] J. K. Eaton and J. R. Fessler. Preferential concentration of particles by turbulence. *Int. J. Multiphase Flows*, 20:169–209, 1994.
- [14] B. M. Sumer and R. Deigaard. Particle motions near the bottom in turbulent flow in an open channel. Part 2. *J. Fluid Mech.*, 109:311–337, 1981.
- [15] G. A. Kallio and M. W. Reeks. A numerical simulation of particle deposition in turbulent boundary layers. *Int. J. Multiphase Flows*, 15:433–446, 1989.
- [16] J. B. McLaughlin. Aerosol particle deposition in numerically simulated channel flow. *Phys. Fluids*, 1:1211–1224, 1989.
- [17] C. Marchioli and A. Soldati. Mechanisms for particle transfer and segregation in a turbulent boundary layer. *J. Fluid Mech.*, 48:283–315, 2002.
- [18] H. Tabaei Kazerooni, W. Fornari, J. Hussong, and L. Brandt. Inertial migration in dilute and semidilute suspensions of rigid particles in laminar square duct flow. *Phys. Rev. Fluids*, 2: 1–23, 2017.
- [19] M. Hogue, C. I. Calle, P. S. Weitzman, and D. R. Curry. Calculating the trajectories of triboelectrically charged particles using discrete element modeling (dem). *J. Electrostat.*, 66: 32–38, 2008.
- [20] S. Watano, S. Saito, and T. Suzuki. Numerical simulation of electrostatic charge in powder pneumatic conveying process. *Powder Technol.*, 135–136:112–117, 2003.
- [21] P. Z. Kolniak and R. Kuczynski. Numerical modeling of powder electrification in pneumatic transport. *J. Electrostat.*, 23:421–430, 1989.
- [22] K. Tanoue, A. Ema, and H. Masuda. Effect of material transfer and work hardening of metal surface on the current generated by impact of particle. *J. Chem. Eng. Jpn.*, 32:544–548, 1999.

- [23] K. Tanoue, H. Tanaka, H. Kitano, and H. Masuda. Numerical simulation of triboelectrification of particles in a gas-solid two-phase flow. *Powder Technol.*, 118:121–129, 2001.
- [24] E. W. C. Lim, J. Yao, and Y. Zhao. Pneumatic transport of granular materials with electrostatic effects. *AIChE J.*, 58(4):1040–1059, 2012.
- [25] H. Grosshans and M. V. Papalexandris. Direct numerical simulation of triboelectric charging in a particle-laden turbulent channel flow. *J. Fluid Mech.*, 818:465–491, 2017.
- [26] H. Grosshans and M. V. Papalexandris. Large eddy simulation of triboelectric charging in pneumatic powder transport. *Powder Technol.*, 301:1008–1015, 2016.
- [27] L. Villafañe, A. Banko, C. Elkins, and J. K. Eaton. Gas heating by radiation absorbing inertial particles in a turbulent duct flow. In *Annual Research Briefs*, Center for Turbulence Research, Stanford University, USA, 2017.
- [28] S. Elgobashi. On predicting particle-laden turbulent flows. *Appl. Sci. Res.*, 52:309–329, 1994.
- [29] J. P. Boris, F. F. Grinstein, E. S. Oran, and R. L. Kolbe. New insights into large eddy simulation. *Fluid Dyn. Res.*, 100:199–228, 1992.
- [30] G. S. Jang and C. W. Shu. Efficient implementation of weighted ENO schemes. *J. Comput. Phys.*, 126:202–228, 1996.
- [31] J. Gullbrand, X. S. Bai, and L. Fuchs. High-order Cartesian grid method for calculation of incompressible turbulent flows. *Int. J. Num. Meth. Fluids*, 36:687–709, 2001.
- [32] H. Grosshans and M. V. Papalexandris. On the accuracy of the numerical computation of the electrostatic forces between charged particles. *Powder Technol.*, 322:185–194, 2017.
- [33] H. Grosshans. Modulation of particle-laden flows by electrostatic charges. In *12th International Symposium on Hazards, Prevention and Mitigation of Industrial Explosions*, Kansas City, MO, USA, 2018. submitted.
- [34] F. V. Bracco. Modeling of Engine Sprays. *SAE Tech. Pap.*, 850394, 1985.
- [35] L. Schiller and A. Z. Naumann. A drag coefficient correlation. *Z. Ver. Dtsch. Ing.*, 77: 318–320, 1933.
- [36] G. Stiesch. *Modeling Engine Spray and Combustion Processes*. Springer Verlag, Berlin Heidelberg New York, 2003.
- [37] H. Grosshans and M. V. Papalexandris. Evaluation of the parameters influencing electrostatic charging of powder in a pipe flow. *J. Loss Prev. Process Ind.*, 43:83–91, 2016.
- [38] H. Grosshans and M. V. Papalexandris. A model for the non-uniform contact charging of particles. *Powder Technol.*, 305:518–527, 2016.
- [39] H. Grosshans and M. V. Papalexandris. Numerical study of the influence of the powder and pipe properties on electrical charging during pneumatic conveying. *Powder Technol.*, 315: 227–235, 2017.
- [40] Z. Zhu, H. Yang, and T. Chen. Direct numerical simulation of turbulent flow in a straight square duct at Reynolds number 600. *J. Hydrodyn.*, 21:600–607, 2009.
- [41] L. Prandtl. Bericht über die Entstehung der Turbulenz. *Z. Angew. Math. Mech.*, 5:136–139, 1925.
- [42] T. von Kármán. Mechanische Ähnlichkeit und Turbulenz. In *Proc. 3rd Int. Congr. Applied Mechanics*, pages 85–105, Stockholm, 1930.

- [43] J. Kim, P. Moin, and R. Moser. Turbulence statistics in fully developed channel flow at low Reynolds number. *J. Fluid Mech.*, 177:133–166, 1987.
- [44] R. Brück. Chemische Konstitution und elektrostatische Eigenschaften von Polymeren. *Kunststoffe*, 71:308–312, 1981.
- [45] W. John, G. Reischl, and W. Devor. Charge transfer to metal surfaces from bouncing aerosol particles. *J. Aerosol Sci.*, 11(2):115–138, 1980.
- [46] T. Matsuyama. A discussion on maximum charge held by a single particle due to gas discharge limitation. In *AIP Conference Proceedings*, volume 1927. American Institute of Physics, 2018.
- [47] T. Matsuyama and H. Yamamoto. Charge relaxation process dominates contact charging of a particle in atmospheric conditions. *J. Phys. D: Appl. Phys.*, 28:2418–2423, 1995.
- [48] T. Matsuyama and H. Yamamoto. Charge relaxation process dominates contact charging of a particle in atmospheric conditions: II. The general model. *J. Phys. D: Appl. Phys.*, 30: 2170–22175, 1997.
- [49] T. Matsuyama, M. Ogu, H. Yamamoto, J. C. M. Marijnissen, and B. Scarlett. Impact charging experiments with single particles of hundred micrometre size. *Powder Technol.*, 135–136: 14–22, 2003.
- [50] A. Noorani, R. Vinuesa, L. Brandt, and P. Schlatter. Aspect ratio effect on particle transport in turbulent duct flows. *Phys. Fluids*, 28(11):115103, 2016.